TU Delft

Delft University of Technology

# Parametric Curve Comparison for Modeling Floating Offshore Wind Turbine Substructures

Ojo, Adebayo; Collu, Maurizio; Coraddu, Andrea

**DOI**
10.3390/en16145371

**Publication date**
2023

**Document Version**
Final published version

**Published in**
Energies

**Citation (APA)**
Ojo, A., Collu, M., & Coraddu, A. (2023). Parametric Curve Comparison for Modeling Floating Offshore Wind Turbine Substructures. *Energies*, *16*(14), Article 5371. https://doi.org/10.3390/en16145371

**Important note**
To cite this publication, please use the final published version (if applicable).
Please check the document version above.

**Copyright**
Other than for strictly personal use, it is not permitted to download, forward or distribute the text or part of it, without the consent of the author(s) and/or copyright holder(s), unless the work is under an open content license such as Creative Commons.

**Takedown policy**
Please contact us and provide details if you believe this document breaches copyrights.
We will remove access to the work immediately and investigate your claim.

*This work is downloaded from Delft University of Technology.*
*For technical reasons the number of authors shown on this cover page is limited to a maximum of 10.*

*energies*

MDPI

*Article*

# Parametric Curve Comparison for Modeling Floating Offshore Wind Turbine Substructures

**Adebayo Ojo [1], Maurizio Collu [1,*] and Andrea Coraddu [2]**

[1] Department of Naval Architecture Ocean and Marine Engineering, University of Strathclyde, Glasgow G4 0LZ, UK; adebayo.ojo@strath.ac.uk
[2] Department of Maritime & Transport Technology, Delft University of Technology, 2628 CD Delft, The Netherlands; a.coraddu@tudelft.nl
* Correspondence: maurizio.collu@strath.ac.uk

**Abstract:** The drive for the cost reduction of floating offshore wind turbine (FOWT) systems to the levels of fixed bottom foundation turbine systems can be achieved with creative design and analysis techniques of the platform with free-form curves to save numerical simulation time and minimize the mass of steel (cost of steel) required for design. This study aims to compare four parametric free-form curves (cubic spline, B-spline, Non-Uniform Rational B-Spline and cubic Hermite spline) within a design and optimization framework using the pattern search gradient free optimization algorithm to explore and select an optimal design from the design space. The best performance free-form curve within the framework is determined using the Technique for Order Preference by Similarity to Ideal Solution (TOPSIS). The TOPSIS technique shows the B-spline curve as the best performing free-form curve based on the selection criteria, amongst which are design and analysis computational time, estimated mass of platform and local shape control properties. This study shows that free-form curves like B-spline can be used to expedite the design, analysis and optimization of floating platforms and potentially advance the technology beyond the current level of fixed bottom foundations.

**Keywords:** FOWT; design; optimization; parametric free-form; TOPSIS

check for updates

**Citation:** Ojo, A.; Collu, M.; Coraddu, A. Parametric Curve Comparison for Modeling Floating Offshore Wind Turbine Substructures. *Energies* **2023**, *16*, 5371. https://doi.org/10.3390/en16145371

Academic Editors: Rafael Campos Amezcua and Erasmo Cadenas

Received: 13 May 2023
Revised: 7 July 2023
Accepted: 11 July 2023
Published: 14 July 2023

**Copyright:** © 2023 by the authors. Licensee MDPI, Basel, Switzerland. This article is an open access article distributed under the terms and conditions of the Creative Commons Attribution (CC BY) license (https://creativecommons.org/licenses/by/4.0/).

## 1. Introduction and Background

Floating offshore wind turbines (FOWT) are an innovative technology currently being embraced to explore the vast resources of the ocean (wind and hydrogen) in the push for net zero carbon emissions. However, the most matured technology in the offshore wind turbine (OWT) sector is the fixed bottom foundation [1], which leaves the concept of the floating offshore wind turbine in the pre-commercial stage in spite of it being proposed by Heronemus over half a century ago in 1972 [2]. Despite the early interest in the floating offshore wind turbine (FOWT) sector, the technology is still yet to maximize its potential. The oil and gas industry's three basic floating platform concepts—spar, semisubmersible and tension leg platforms—remain the main platform configurations in the FOWT sector. Bringing the cost of the substructure used in the FOWT system down to the level of the fixed bottom platform requires an extensive developmental process. This study aims to explore and compare the use of several parametric free-form curves to support a bespoke design and optimization methodology for a spar FOWT system using the multi-criteria decision making (TOPSIS) technique. The innovative shapes generated for the optimal designs due to the local control property of the free-form curves sets this study apart from others where the global dimension of the design is altered, i.e., the entire length or diameter of the platform changes rather than there being local changes in diameter at the control points. The TOPSIS technique uses weighted criteria (computational time, platform mass, local control properties of free-form curve, parametric continuity and nacelle acceleration estimates). This will essentially give different perspective to designers to save costs and time and to deliver innovative platform concepts as the FOWT sector gradually moves

into the commercial phase of development. The parametric curves compared in this study are the cubic spline, cubic Hermite spline (CHS), B-spline and the Non-Uniform Rational B-spline.

Developing new floater concepts to improve performance and reduce the overall cost of an FOWT system is conducted by considering the two state-of-the-art techniques highlighted below and reviewed in Sections 1.1 and 1.2, respectively.

1. Shape Parameterization Technique;
2. Design, Analysis and Optimization Technique.

Selecting the best free-form curve for the shape parameterization technique is conducted by the Multi-Criteria Decision Making (MCDM) techniques and reviewed in Section 1.3.

### 1.1. Shape Parameterization Review

The concept of parameterization has been used in many engineering and design sectors, including the floating offshore wind sector, as highlighted in Tracy [3], where they presented a study that describes the system coupling and dynamic analysis of floating wind turbine support structures that enable a parametric design of the floating wind turbine concepts and the mooring systems. The parameterization technique used for the platform type is to vary the global diameter and draft of the platform. Their findings demonstrate that, when considering the wind and sea state environmental conditions, the Pareto optimal structures for a system coupled dynamic analysis of the turbine, the tower and the FOWT substructure (floater, mooring lines and anchors) are typically either a shallow barge with concrete ballast or a lengthy draft spar.

Rahmdel et al. [4] conducted a parametric study of spar-type FOWTs by numerical investigations with the aim of conducting dynamic response analysis and developing design guidelines for spar FOWTs. They numerically obtained the dynamic responses of full-scale spar-type FOWT models with three main design variables (spar diameter, depth and concrete ratio) in the time domain. They then experimentally validated their results by factoring in environmental conditions like wind, regular wave, constant current loads and the mooring line loads. They then conducted regression and perturbation analyses validated by the analysis of variance method to analyze the effects of the design variables and to propose design guidelines of spar-type FOWTs.

Hegseth et al. [5] conducted a design optimization of an integrated platform, tower, mooring system and blade pitch controller for a 10 MW spar floating wind turbine system. The design parameters for the spar in this study are the diameter and wall thickness along the length of the platform in ten different sections including the dimensions of the stiffeners, which were modeled using a B-spline curve with four control points. The study shows that the optimized platform's diameter is relatively small in the wave zone and has an hourglass shape far below the waterline. This design limits the wave loads on the structure. The shape increases the restoring moment and natural frequency in pitch, which results in an improved dynamic response in the low-frequency range.

Birk [6] developed an optimization framework that interfaces a design tool for geometric shape parameterization, a potential theory analysis tool for 3D diffraction-radiation analysis and a hydrodynamic performance assessment tool for short- and long-term wave statistics. In this framework, the algorithm alters a set of selected shape parameters to minimize the substructure's motions and force the satisfaction of the system's safety design requirements. The constraints used within their framework ensure that only feasible designs with the required stability in operation and survival conditions are selected.

In the offshore shipping and marine sector, Katsoulis et al. [7] developed a T-splines-parametric modeller (TshipPM) for bespoke and convoluted ship designs. The TshipPM offers the flexibility needed to represent complex ship-hull geometry features including the bow, stern and geometric change zones from the ship's center to the forward and backward perpendiculars. The T-Ship is capable of providing these complex smooth geometric shapes at minimal cost in comparison with the parametric modelers like NURBS free-form curves.

### 1.2. Design, Analysis and Optimization Review

Design analysis and optimization are central to many engineering disciplines, including disciplines within the offshore sector. The floating offshore wind turbine is a multidisciplinary system comprising the aerodynamics, structural, servo-dynamics and hydrodynamics disciplines. A couple of Multidisciplinary Design Analysis and Optimization (MDAO) studies conducted in the offshore sector including FOWT studies are highlighted herein.

A good summary review of design, analysis and optimization studies is provided in Table 1, with more details of the optimization framework in the references for the readers.

**Table 1.** Summary of FOWT Platform Optimization Review.

| Optimization Type | Algorithm | Platform | Reference |
|---|---|---|---|
| GF | GA | Spar; Semi-submersible; TLP | Hall et al. [8] |
| GF | Bat (BA) | Spar; Semi-submersible; TLP | Karimi et al. [9] |
| GF | GA | New concept | Ramsay et al. [10] |
| GB | SQP | Spar | Dou et al. [11] |
| GF | GA | Spar | Ojo et al. [12] |

### 1.3. Multi-Criteria Decision Method

Multi-criteria decision making (MCDM) techniques are useful tools for decision makers faced with selecting options in situations where there are multiple, often conflicting, criteria to consider [13]. These techniques allow decision makers to evaluate the options based on multiple criteria simultaneously, which can lead to more informed and effective decision making. Caylor and Hanratty [13] conducted a survey of seven state-of-the-art MCDM methods, amongst which are the Weighted Sum Model (WSM), Analytical Hierarchy Process (AHP), Technique for Order of Preference by Similarity to Ideal Solution (TOPSIS), Preference Ranking Organization METHod for Enrichment of Evaluations (PROMETHEE), VlseKriterijumska Optimizacija I Kompromisno Resenje (VIKOR), elimination et choix traduisant la realité (ELECTRE) and Reference Ideal Method (RIM). Their survey concluded that selecting a suitable method can be challenging.

As highlighted in Roszkowska [14], some of the exceptional attributes of the TOPSIS MCDM technique amongst other MCDM techniques are: simplicity, rationality, comprehensibility, good computational efficiency and the ability to measure the relative performance for each alternative in a simple mathematical form. These properties make it suitable for engineering design (FOWT support structures inclusive). The use of TOPSIS in the offshore wind and floating offshore wind sector are detailed in [15–18]. Based on the highlighted properties of TOPSIS, the comparison of the free-form curves within the design and optimization framework in this study is conducted with the TOPSIS technique.

### 1.4. Contribution to Research

This study addresses the use of free-form curves within an MDAO framework to design an FOWT platform and ranks the best performance curve using a robust MCDM technique—TOPSIS. The contributions are highlighted herein:

1. The study shows innovative ways of coming up with bespoke designs that are fit for purpose. This stems from the stochastic iterations of set boundary design parameters (radii) that are systematically passed into the control points of a free-form curve with local propagation properties to vary the geometric shape of an FOWT platform within a MDAO framework, which is a novelty in the FOWT sector.
2. Reduces the mass of steel required to manufacture the platform of an FOWT. This leads to a reduction in the capital expenditure of an FOWT project.
3. Demonstrates the capability of reducing computation time with the platform design analysis and optimization framework.

### 1.5. Organization of Article Contents

The structure of this study is highlighted herein—Section 1 provides an introduction to FOWT technology and also describes the aim and objective of this study. In addition, Section 1 highlights a background literature review of the shape parameterization, design, analysis and optimization concept and the multi-criteria decision matrix using the TOPSIS technique that will form the framework of the methodology of this study. Section 2 provides an overview of the four free-form curves to be ranked within the optimization framework. Section 3 highlights the methodology deployed for this study. Section 4 details the simulation, analysis and results of the work conducted. Section 5 provides a detailed conclusion and future recommendations for research.

## 2. Free-Form Curves

### 2.1. Parametric Representation

The parametric description is the most suitable representation for a free-form geometry. The x, y and z coordinates are explicit functions of an independent parameter (or two independent parameters for surfaces). This representation offers the widest range of potential geometries and is very flexible to adopt for design purposes, as it has the capability to define space curves rather than defining curves on planes like the implicit and explicit representation. The independent parameter, often represented as t, i.e., $x = x(t)$, $y = y(t)$, $z = z(t)$ is specified in the range $a \leq t \leq b$ and usually normalized to [0, 1] [19].

This study will evaluate four parametric representations of curves for modeling an FOWT platform. The four curves are the cubic spline, the CHS (which is a variation of the cubic spline), the B-Spline, and the Non-Uniform Rational B-Spline (NURBS).

#### 2.1.1. Cubic Spline

A cubic spline is a piecewise cubic function that interpolates a set of data points and guarantees smoothness at the interpolated points [20]. For a cubic spline, every point where two polynomials meet results in the equality of the first and second derivatives to ensure a smooth fitting line.

A detailed mathematical construction of a cubic spline curve for interpolation and geometry design is presented in Biran [21].

Some properties of the piecewise cubic spline are highlighted herein:

- The piecewise cubic polynomial function interpolates all data points on the geometric curve and guarantees smoothness at the data points.
- The piecewise cubic polynomial function is continuous. It has both slope continuity (C1) and curvature continuity (C2).
- The cubic spline doesn't work well in scenarios when the data points are close together and have extreme differences in value. This is because the cubic spline utilizes slope calculations (change over distance) to figure out the shape of the curve along the design model.

#### 2.1.2. Cubic Hermite Curve

The CHS is a curve in which each piece is a third-degree polynomial specified in the Hermite form. This is defined by its values and first derivatives at the end points of the associated parametric domain interval. It is conceptually the simplest of the parametric curves with slope continuity C1 interpolants, although not the most practical one, as reported by Farin [22].

The CHS is commonly used to construct interpolation curves in engineering modelling and designs for providing solutions to practical engineering problems [22,23].

Some of the properties of the CHS are highlighted below:

- The CHS is readily available and simple to use for engineering models;
- It has a local propagation property which allows the designer to locally control the shape of the curve at the control points;

- As a result of its slope/$C^1$ continuity, it lacks accuracy in representing some common engineering curves like the elliptical arc, circular arc, quadratic parabolic arc, astroid arc and cubic parabolic arc.

#### 2.1.3. B-Spline

A basis spline, often known as a B-spline, is a piecewise polynomial function with unique characteristics that specify the degree/order of the polynomial [22]. The B-spline curve is capable of determining a unique polynomial representation of a set of data which might be for structural points in 3D space or a set of data on a graph.

A B-spline curve is a linear combination of control points $\overline{P}_i$ and B-spline basis function $N_{i,k}$ as highlighted in Equation (1).

$$\overline{R}_{(U)} = \sum_{i=1}^{n} \overline{P}_i N_{i,k}(U) \quad (1)$$

where $\overline{P}_i$ are the control points for the B-spline, k is the order and $N_{i,k}(U)$ is the ith B-spline basis function of order *k*.

The B-spline curve has good properties that make it favorable among engineers for design purposes. Some of the properties are:

- The curve has local propagation properties which make it possible to locally alter the shape of the design rather than altering the entire shape as with curves like the Bezier curve;
- The B-spline curve is invariant under affine transformation;
- The B-spline curve has partition of unity properties;
- The number of segments in a B-spline curve is derived from the degree and the number of control points in the curve, i.e., the number of segments is $n - k + 2$ where n is the number of control points and k is the degree/order of the curve;
- The continuity of the B-spline curve can go beyond the C2/curvature continuity to ensure a higher level of smoothness of the curve. A B-spline curve is $C^{(k-2)}$ continuous;
- A given control point influences 1 or 2 or K curve segments. This ensures the B-spline's localized shape control property.

#### 2.1.4. Non-Uniform Rational B-Spline (NURBS)

The NURBS is at the forefront of several CAD systems in the academic and commercial modeling sector for geometric designs as it has the capability to describe analytic and freeform shapes [24]. Although a B-spline representation is useful for representing freeform shapes, implicit conic sections cannot be effectively modeled with it. This shortcoming can be fixed with the NURBS, which is a new kind of B-spline [22]. The majority of implicit parametric curves can be accurately represented by the NURBS [22,25], as highlighted in Equation (2).

$$\overline{R}_{(U)} = \frac{\sum_{i=1}^{n} \overline{P}_i W_i N_{i,p}(u)}{\sum_{i=1}^{n} W_i N_{i,p}(u)} \quad (2)$$

where $\overline{P}_i$ represents the control points, $N_{i,p}(u)$ is the ith B-spline basis function of order p and $W_i$ represents the weights.

Some properties/attributes of NURBS curves are detailed in Dimas and Briassoulis [24] and highlighted herein:

- Evaluation of the NURBS curve is straightforward, fast and computationally stable;
- They offer similar mathematical representation for free-form surfaces and commonly used analytical shapes such as natural quadrics, extruded surfaces and surfaces of revolution;
- They are invariant under affine (rotation, scaling, translation) transformation as well under shear transformations;
- It is simple to alter the shape of design from NURBS curves through the manipulation of control points, weights and knots;

- Poor weight selection can result in inaccurate curve/surface parameterization;
- The classification of point members is a challenging problem for parametric surfaces; hence, including NURBS as nodes to a constructive solid geometry system is particularly difficult.

## 3. Methodology

The process adopted in selecting the optimum parametric curve for modeling an FOWT substructure in this study is split into two phases:

1. Integrate the parametric curves in the MDAO framework developed by Ojo et al. [12] using the DNV suite software (Sesam GeniE 64 V8.4-06 and HydroD 64 v6.1-02) and the derivative free pattern search optimization algorithm;
2. Adopt a multi-criteria decision making (MCDM) process, more specifically a TOPSIS approach, to rank the parametric curve techniques against established marking criteria.

### *3.1. Integrating Parametric Curves with the MDAO Framework*

The MDAO framework involves an integration of all the multi-disciplines within the FOWT system coupled together, analyzed and benchmarked against the objective function and a set of design and analysis constraints to select the optimal model. The MDAO framework used for this work is detailed in the study conducted by Ojo et al. [12] and summarized in this section.

It involves the definition of a parameterization scheme with the free-form curves discussed in Section 2. The next step is to analyze design models iteratively in the design space using low fidelity analytic tools like DNV WADAM. The second-to-last step is the search and selection of optimal design within the design space by integrating the analysis with the recommended optimizer (derivative-free Pattern Search optimization algorithm). Finally, a multi-criteria decision making process assessment is conducted on the different parametric curves to rank them in the order of modeling durability. The framework described is shown in Figure 1.

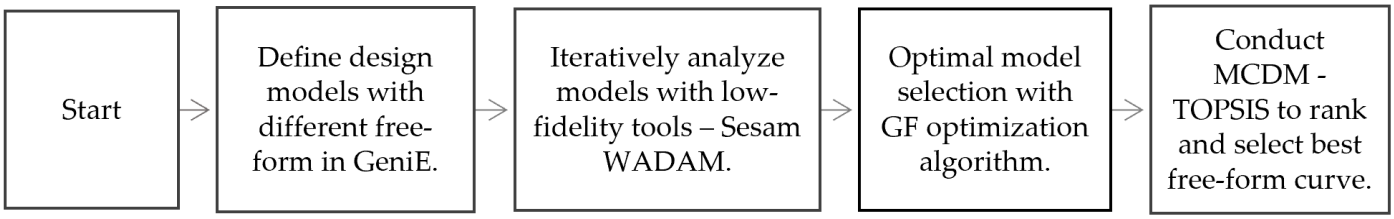


**Figure 1.** Parametric curve and MDAO framework.

### *3.2. Multi-Criteria Decision Making (MCDM) Process—TOPSIS Method*

The TOPSIS method was pioneered by Hwang and Yoon [26]. The method was developed based on the concept that the optimal alternative should have the shortest distance from the positive ideal solution and the longest distance from the negative ideal solution [15,18,26]. This method is used in this study for benchmarking the parametric free-form curve/spline modeling techniques for the FOWT substructure. The TOPSIS flowchart is presented in Figure 2.

Details of the TOPSIS process highlighted in Figure 2 are presented in Appendix A. The TOPSIS process as applied to this study is a systematic approach that helps the designer in identifying the order of performance of the different modeling curves based on unique sets of criteria detailed in Section 4.4.5.

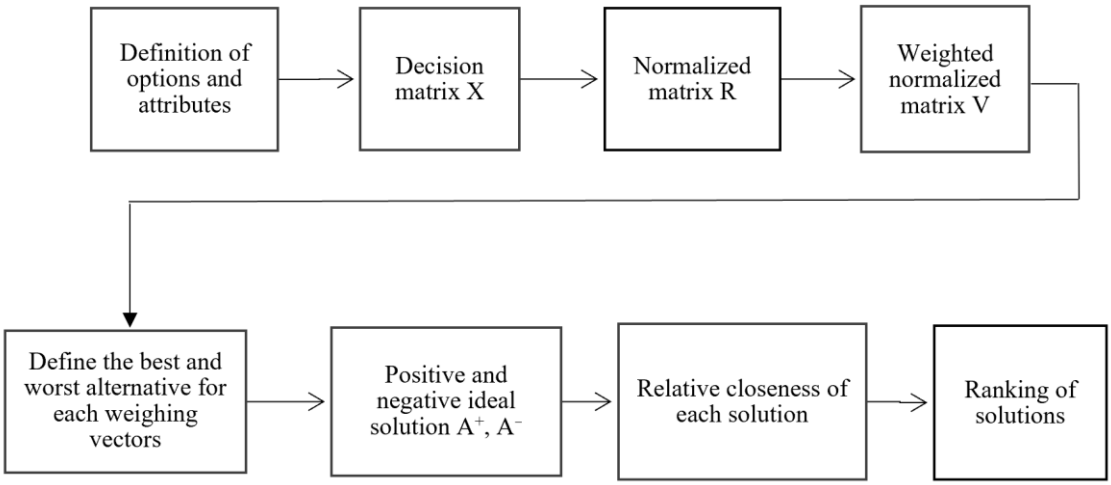


**Figure 2.** TOPSIS process.

## 4. Optimized Models, Results and Discussion

### *4.1. Overview*

This section details the design and analysis technique and optimization process conducted to explore the design space. The baseline substructure is the OC3 5 MW substructure. This work is based on the MDAO framework developed in Ojo et al. [12]. However, in Ojo et al. [12], a B-spline free-form curve was used to model the OC3 5 MW spar with a total of 13 control points and 12 curve segments. For this study, a reduced number of control points (6 control points and 5 curve segments), with different parametric free-form curves, is used. The OC3 spar is basically made of two cylinders connected by a truncated cone at the sea water level. The geometry and structural properties that make up the OC3 spar-buoy are shown in Tables 2 and 3.

**Table 2.** Geometric parameters for OC3 Spar-buoy [27].

| Parameters | Dimensions (m) |
|---|---|
| Top cylinder diameter | 6.5 |
| Height of top cylinder | 4 |
| Diameter at top of transition area | 6.5 |
| Diameter at base of transition area | 9.4 |
| Height of transition area | 8 |
| Bottom cylinder diameter | 9.4 |
| Bottom cylinder height | 108 |
| Base of bottom cylinder to base of tower base (Draft) | 120 |

**Table 3.** Floating platform structural properties [27].

| Parameters | Values per Literature |
|---|---|
| Platform mass (including ballast)—(kg) | 7,466,330 |
| Center of mass below sea water level (SWL)—(m) | 89.9155 |
| Platform roll inertia—about center of mass—kgm$^2$ | 4,229,230,000 |
| Platform pitch inertia—about center of mass—kgm$^2$ | 4,229,230,000 |
| Platform yaw inertia—about central axis—kgm$^2$ | 164,230,000 |

Environmental Parameters

An extreme sea state (DLC1.6a) was used to conduct the global response assessment in this study. The wave spectrum is defined with the irregular JONSWAP spectrum. The sea-state for the site is as used in Leimeister et al. [28], and a water depth of 320 m is considered.

### *4.2. Design and Analysis (Potential Flow Theory)*

In this study, the OC3 5 MW Spar platform's external wet geometry, center of gravity, moments of inertia and radii of gyration are modeled with the DNV Sesam GeniE 64 V8.4-06 software package, and a potential flow-based hydrodynamic analysis is conducted with DNV Sesam HydroD 64 v6.1-02. Sesam GeniE has a large collection of explicit, implicit and parametric free-form curves to enable the creation of design models. Some of these tools are polycurves, cubic splines, CHS, B-splines and NURBS. HydroD tools are utilized for the computation of hydrostatics and stability, wave loads and motion response for the FOWT substructure [29].

The hydrodynamic forces comprise radiation forces and wave excitation forces (including diffraction forces and Froude–Krylov forces). The formulation for the radiation and diffraction boundary value problem and the resulting hydrodynamic added mass, damping matrices and wave excitation force depends on water depth, frequency and the geometric shape of the support platform and its proximity to the free surface. Also, the direction of the incident waves affects the wave excitation [30]. In the frequency domain approach, the platform motions are assumed to be at the same frequency as the incident waves, which are regular waves. Although this prevents the system's transient responses from being modelled, the linearity assumption allows the responses at various wave frequencies to be superimposed according to a wave spectrum to predict the system's behavior in random sea states [8]. A detailed study of the potential flow theory and the equations of motion in regular waves that govern the frequency domain approach and also the computation of response amplitude operators in different degrees of freedom is available in the literature [31,32].

### *4.3. Optimization, Objectives and Constraints*

The meta-heuristic PSM is the optimizer used in this geometric shape parameterized modeling framework using different free-form curves (cubic spline, CHS, B-spline and NURBS). PSM is selected for this study because it has a global convergence property, which prevents stagnation in the local minimum because it presents an exhaustive search throughout the exploration and exploitation process [33].

The single objective for this MDAO study is to minimize the cost of steel required for the design and manufacture of the spar-buoy platform. This translates to minimizing the mass of steel needed in manufacturing the platform. The constraints considered for all the parametric free-form curves considered in this study are highlighted below:

1. The maximum static pitch angle of inclination of the system does not exceed 5 degrees;
2. A positive ballast mass to ensure floatability;
3. Nacelle acceleration not more than 20–30% of gravitational acceleration.

The formulation of the optimization problem is described as shown in Equation (3).

$$\min_{x \in \mathbb{R}} J(x) \quad \text{subject to} \begin{cases} x_{lower} \leq x \leq x_{upper} \\ h_i(x) = 0;\ i = 1 \text{ to } m \\ g_i(x) \leq 0;\ j = 1 \text{ to } p \end{cases} \tag{3}$$

where x is an n-dimensional vector of design variables with lower and upper boundary values, $J(x)$ is a single objective function, m represents equality constraints and p represents inequality constraints.

In this study, 'x' represents the varying diameter along the free-form curve used to model the spar. The objective is to minimize the mass of steel which is influenced by the

diameter along the free-form curve. The main inequality constraint is the static pitch angle less than or equal to 5 degrees and the nacelle acceleration value of less than 2.943 $m/s^2$.

### *4.4. Results*

#### 4.4.1. Overview

The results from this study are split into three sections highlighted below.

The first section discusses the parametric curve modeling of the OC3 platform with few control points (six control points and five segments), estimating the mass and the system's response from models of parametric curves using the OC3 dimension [27].

The second section discusses the shape variation and optimization with the MDAO framework, estimating the system's response using the developed MDAO framework for all the parametric curves discussed in this article. All optimized curves yielded different shapes according to the specified constraints and objective function.

The third section discusses the ranking of the parametric curves, employing the TOPSIS methodology to rank the best performing curve for the design based on selected performance criteria.

#### 4.4.2. Parametric Curves Modeling and Analysis with OC3 Dimension

The first result section shows the evaluation of the system's response (nacelle acceleration) and the estimated mass of steel utilized in the design for the free-form parametric modeling curves used with the dimension of the OC3 platform. This estimate has been conducted for the parametric curve used within the MDAO framework conducted in Ojo et al. [12]. The present analysis goes further by assessing the estimated mass of steel and nacelle acceleration response from other parametric modeling curves (cubic spline, CHS, B-spline and NURBS) using the sea state shown in Table 4. The data for the design model's parametric curves considered are presented in Table 5. The number of control points is reduced to six, as highlighted in Table 5, in order to reduce the dimensionality of the design space investigated by the MDAO framework. A comparison of the parametric curves on the OC3 design model with a plot of the design data points in Table 5 is presented in Figure 3. It is shown in Figure 3 that all the parametric curves on the model are smooth curves with higher continuity in comparison to the OC3 data plots from Table 5.

**Table 4.** Sea state and environmental data for site [28].

| **Wind and Wave Properties** | | |
|---|---|---|
| $H_s$ (m) | 10.37 | Significant wave height of the spectrum |
| $T_p$ (s) | 14.70 | Peak period of the wave spectrum |
| Peak/Gamma factor | 3.30 | Non-dimensional peak shape parameter |
| $\sigma_1$ | 0.07 | Spectral width parameter for angular frequency $\leq$ peak angular frequency |
| $\sigma_2$ | 0.09 | Spectral width parameter for angular frequency > peak angular frequency |
| $U_{ref}$ (m/s) | 12 | Rated wind speed |
| Wind shear exponent | 0.12 | Extreme wind shear exponent |

**Table 5.** OC3 spar-buoy cubic spline, cubic Hermite spline, B-spline and NURBS.

| Height (m)/Control Points | 10 | 0 | −4 | −12 | −60 | −120 |
|---|---|---|---|---|---|---|
| Radius (m) | 3.25 | 3.25 | 3.25 | 4.7 | 4.7 | 4.7 |

The black plot in Figure 3 represents a straight line with no continuity used in plotting the radii coordinates of the standard OC3 spar platform highlighted in Table 5. The black

plot in Figure 3 shows the straight line passing through all the control points highlighted in Table 5 with high accuracy. However, there is no continuity when the direction of the control point changes. The four other curves in Figure 3 from left to right are the cubic spline, CHS, B-spline and NURBS curve modeled according to the OC3 coordinates in Table 5 with various degrees of approximation around the control points. The curves don't pass through the control points representing all the coordinates in Table 5 between the first and last coordinates; hence, they are termed approximation curves. Unlike the black straight-line plot in Figure 3 that passes through all the control point coordinates, the other parametric free-form curves highlighted in blue in Figure 3 are only guaranteed to accurately pass through the first and last control points and they all exhibit a degree of continuity when the control point direction changes.

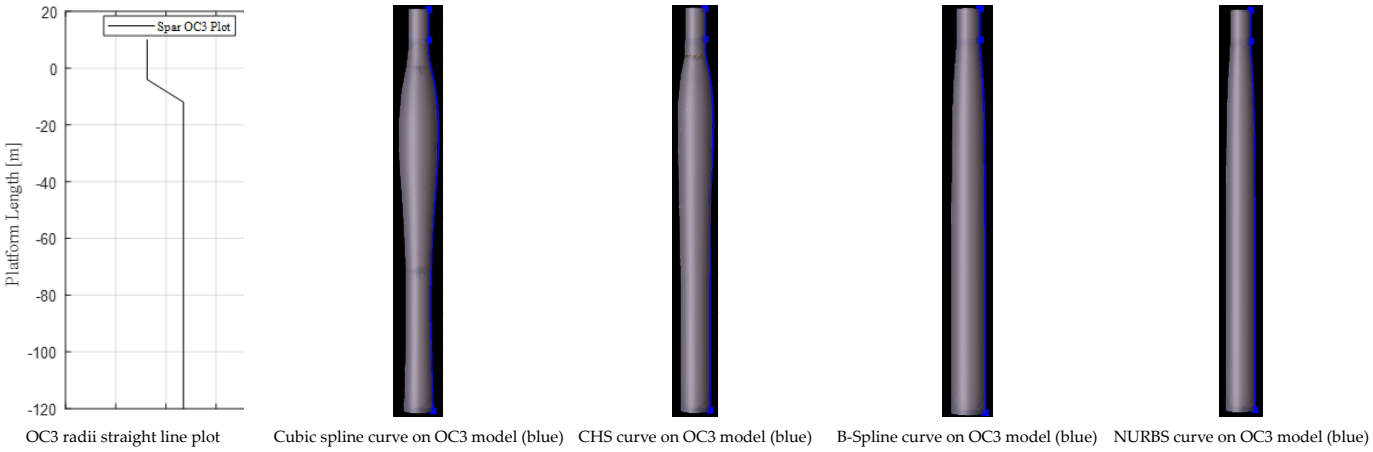


**Figure 3.** Comparison of the parametric curves on OC3 spar model with the plots from the OC3 data points.

The difference in shape of the parametric free-form curves in the blue lines and the OC3 dimension plots in the black lines are due to the unique properties of the free-form curves, amongst which are slope continuity, curvature continuity and the local propagation capabilities of the curve at the control points. A sweep of these curves produces the modeled spar, which represents the wet boundary conditions for hydrostatic and hydrodynamic analysis. A hydrodynamically assessed model of the OC3 spar modeled with the different free-form curves discussed is shown in Figure 4.

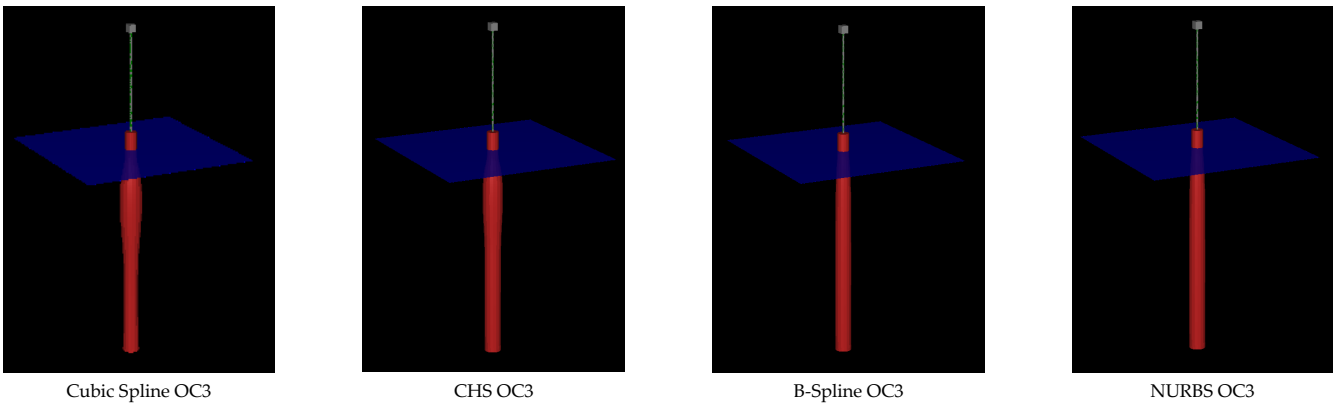


**Figure 4.** Hydrodynamically assessed OC3 shape variants from different spline model.

The hydrodynamic assessment of the modeled platforms highlighted in Figures 3 and 4 are detailed in Section 4.4.3, with the system's surge, heave, pitch and nacelle displacement response assessed with the wave ebergy spectrum in Figure 5 is highlighted in Figure 6.

The estimated mass from the approximate modeling of the OC3 spar using the free-form curves is highlighted in Table 6. The nacelle acceleration calculated from the responses presented in Table 7.

**Table 6.** OC3 dimensioned mass model for the free-form curves.

| Parametric Curve | B-Spline | CHS | NURBS | Cubic Spline |
|---|---|---|---|---|
| Mass (kg) | 1,898,111 | 1,824,997 | 1,890,991 | 1,812,714 |

4.4.3. Wave Spectrum and Response Amplitude Operator Results for OC3 Model

The wave energy spectrum for the site is derived from the data provided in Table 4 and presented in Figure 5, with a peak wave spectrum of 320 $m^2$/Hz at a peak period of 14.7 s.

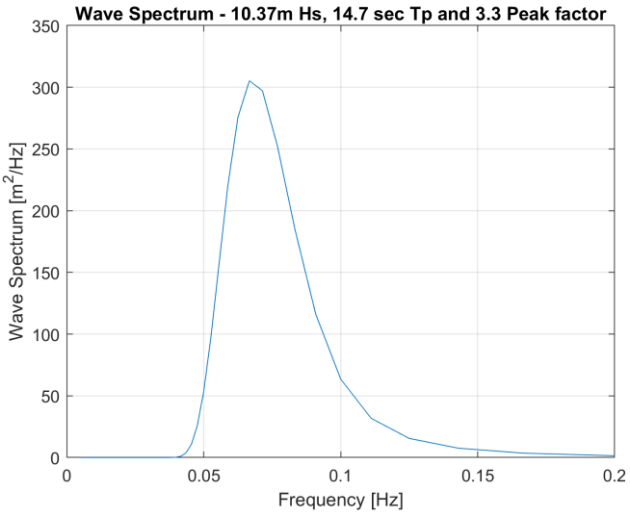


**Figure 5.** Wave spectrum—10.37 m Hs and 14.7 s Tp.

The surge, heave and pitch response amplitude operators for all the free-form models developed from the dimensions in Table 5 are represented in Figure 6.

It is shown in Figure 6 that for the parametric free-form curves and all the degrees of freedom (surge, heave, pitch) assessed, including the nacelle displacement, the peak responses of the NURBS model and the B-spline model appear to be below the range of first-order wave excitation force frequencies (i.e., the region between ~0.04 Hz to ~0.2 Hz) for the surge and pitch degrees of freedom, while the peak frequencies for the cubic spline model and the CHS model are around the boundary of the first-order wave excitation frequency range for the same degrees of freedom. This shows that the models designed with the cubic spline and CHS may have a larger dynamic response than the configurations obtained with the NURBS and the B-spline approaches. However, the heave response peak is outside the first-order wave excitation region for all the approaches.

The same observation is made with the nacelle displacement response. The geometries obtained with the NURBS and the B-spline approaches show the peak response of the nacelle displacement to be outside the first-order wave excitation region, while the peak response of the geometries from the cubic spline and the CHS are within this region, again increasing the likelihood of a larger dynamic response to waves.

The nacelle acceleration of the parametric free-form curves assessed with the OC3 spar-buoy dimension are highlighted in Table 7: the CHS free-form curve has the largest nacelle acceleration of 0.111 m/$s^2$, which is still within the allowable nacelle acceleration value of 20–30% of gravitational acceleration [28].

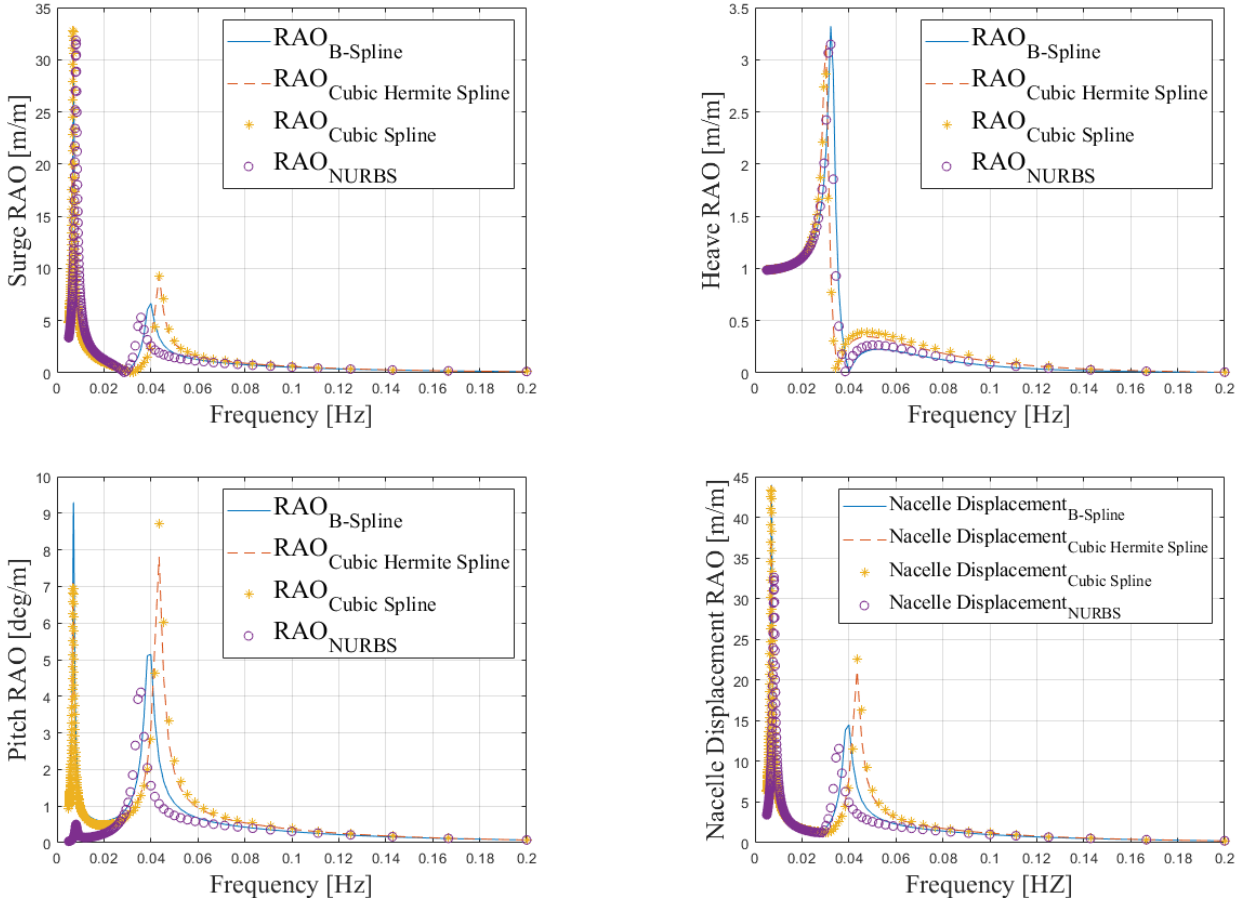


**Figure 6.** Surge, heave, pitch and nacelle displacement RAO for the four parametric curves.

**Table 7.** OC3 Nacelle acceleration RMS for the free-form curves.

| | CS | CHS | B-Spline | NURBS |
|---|---|---|---|---|
| Nacelle Acceleration RMS ($m/s^2$) | 0.1184 | 0.1110 | 0.0842 | 0.0780 |

#### 4.4.4. Shape Alteration and Optimization with MDAO Framework—Optimized Shape and Response Amplitude Operator Results

The Shape Alteration and Optimization Framework (SAOF) is a platform designed to evaluate the performance of different parametric free-form curves that are integrated into the optimization framework in this study. The SAOF allows for the exploration and modification of curves to optimize their shapes and achieve design objectives and goals.

The shape variation and optimization process results in the selection of the optimal design from the parametric curve and the MDAO framework described in Section 3. The objective of the MDAO framework is to minimize the mass of steel used for design, which invariably reduces the capital cost of the spar-buoy platform. Also, the result satisfies the static pitch angle constraint of 5 degrees set for all the four free-form parametric curves assessed. Other constraints set are to ensure a positive ballast, which is a way to impose floatability, and also maintain allowable nacelle acceleration as detailed in Ojo et al. [12]. The results of the optimal shape variants when the objective and constraints are applied to the MDAO framework are discussed in this section. The optimized dimension or data on the varying control points along the different free-form curves are highlighted in Table 8.

**Table 8.** Dimension of optimal shapes B-spline, CHS, NURBS and cubic spline.

| | | | | | | | |
|---|---|---|---|---|---|---|---|
| B-spline | Height (m)/Control Points | 10 | 0 | −4 | −12 | −60 | −120 |
| | Radius (m) | 3.2500 | 4.4265 | 6.3936 | 1.0000 | 6.3405 | 5.7031 |
| CHS | Height (m)/Control Points | 10 | 0 | −4 | −12 | −60 | −120 |
| | Radius (m) | 3.2500 | 4.6989 | 5.2885 | 5.6596 | 2.7773 | 5.3838 |
| NURBS | Height (m)/Control Points | 10 | 0 | −4 | −12 | −60 | −120 |
| | Radius (m) | 3.2500 | 3.3567 | 3.6938 | 6.9297 | 4.2880 | 6.0581 |
| Cubic Spline | Height (m)/Control Points | 10 | 0 | −4 | −12 | −60 | −120 |
| | Radius (m) | 3.2500 | 2.2297 | 5.5297 | 5.7791 | 5.2409 | 2.8487 |

An illustration of the optimal spar variant is shown at the top of Figure 7 with a straight-line plot that passes through all the optimal variant coordinates/control points from all the parametric free-form curves highlighted in Table 8. As discussed in Section 4.4.2, the black plots at the top of Figure 7 show that the straight line plot of the selected parametric free-form curve's optimal variants from Table 8 pass through all the control point highlighted in Table 8 with high accuracy and no degree of continuity when the control point coordinates change direction.

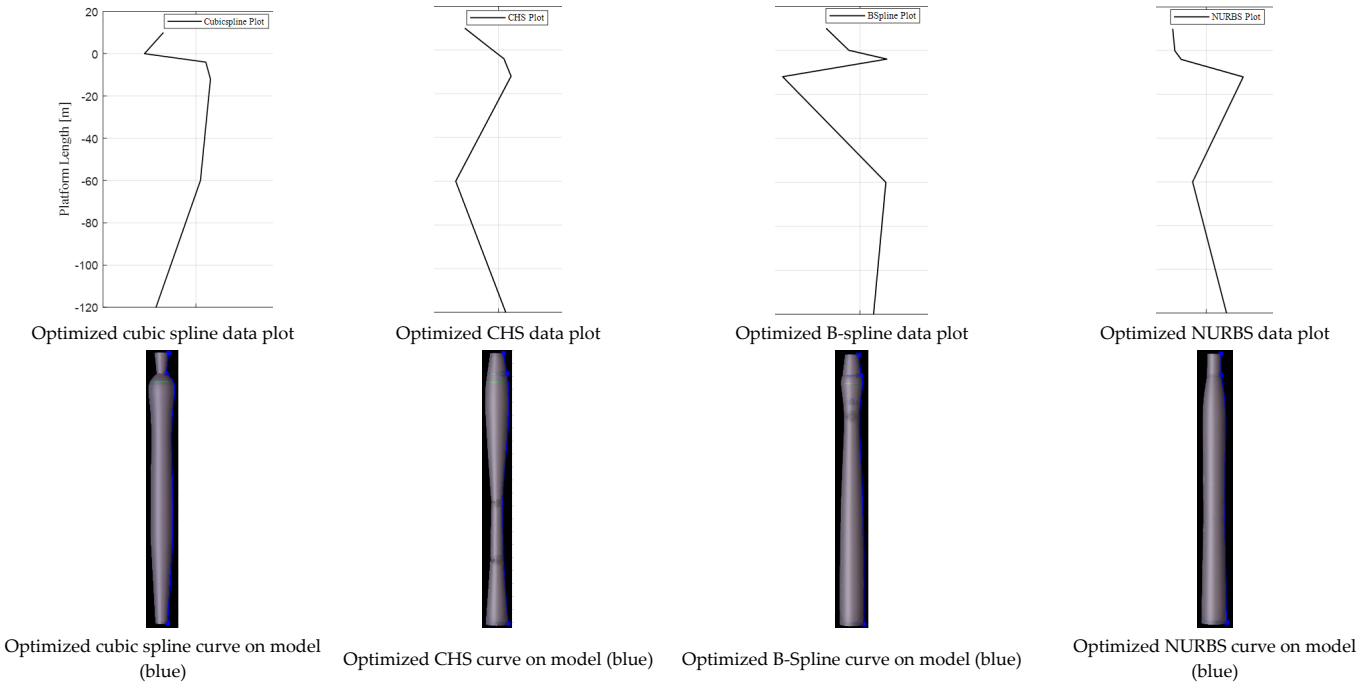


**Figure 7.** Comparison of the optimized shape parametric curves on model with the plots of the curves from the optimized data point along the length of the spar.

The model below in Figure 7 shows the parametric free-form curves in blue from which the models are developed with a curve sweep in Sesam GeniE. As highlighted in Section 4.4.2, the parametric free-form curves used to develop the selected optimized variant from the MDAO framework show unique properties, amongst which are slope continuity, curvature continuity and local propagation properties which ensure a smooth transition when the control point coordinates change direction.

The results for the hydrodynamic motion response in surge, heave, pitch and nacelle displacement of the selected optimized variants shown in Figures 7 and 8 are presented in Figure 9.

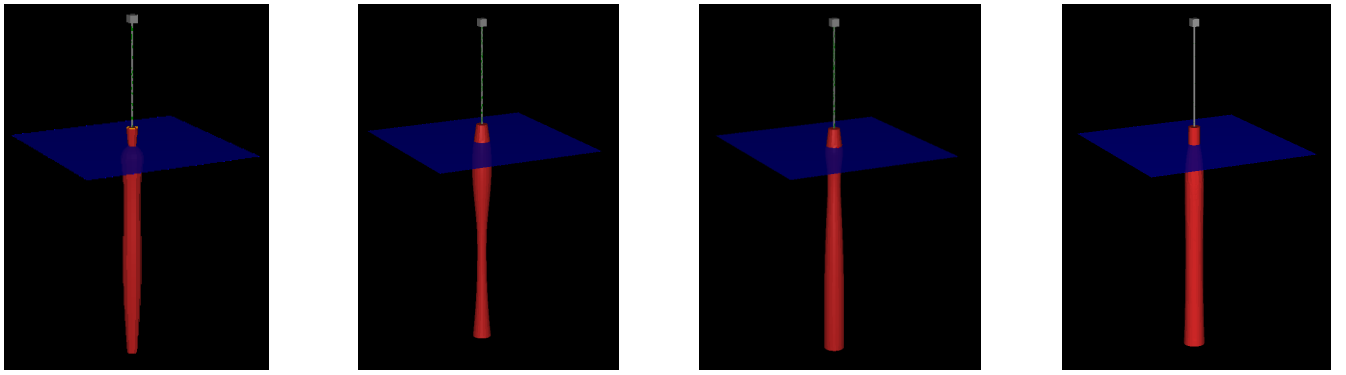

Reduced MDAO optimized cubic spline | Reduced MDAO optimized CHS | Reduced MDAO optimized B-Spline | Reduced MDAO optimized NURBS

**Figure 8.** Optimal shape variants from MDAO framework with different spline models.

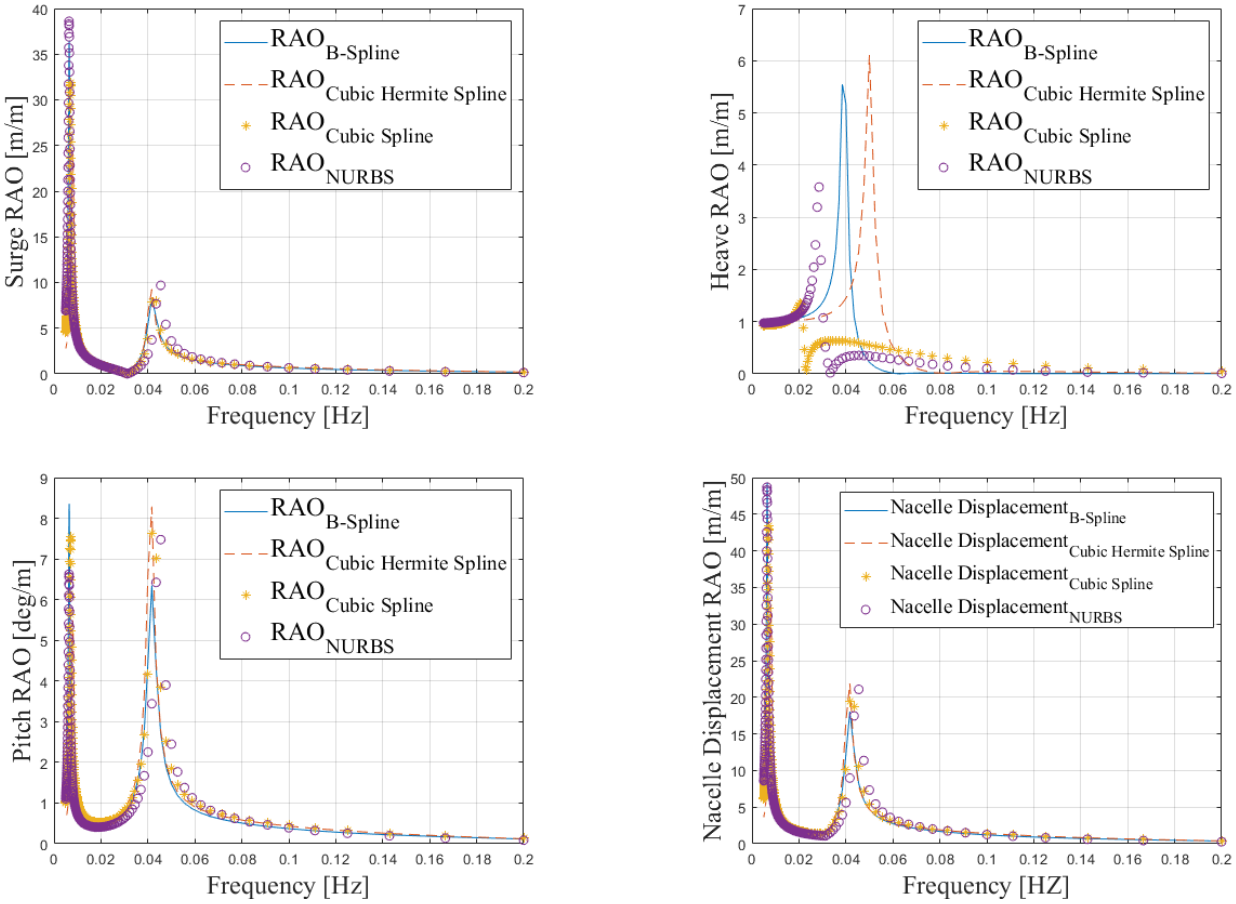


**Figure 9.** Optimal shape variants surge, heave, pitch and nacelle displacement RAO for all four parametric curves.

The response results for the optimal shape variants are presented in Figure 9. The peak response frequency for the surge degrees of freedom, as well as the peak of the nacelle displacement RAO, are well outside the first-order wave excitation range, while the peak response frequency for the pitch degree of freedom is around the boundary of the first-order wave excitation range for all the free-form curves assessed. However, for the heave degree

of freedom, the peak response frequency for the CHS free-form curve is within the first-order wave excitation range, which may lead to a larger dynamic response of this platform to typical sea states, while the same does not happen for the other parameterization curves, whose peaks are outside this region.

The other results assessed for the optimal variants selected from each free-form curve are the mass estimate from the hydrostatic analysis highlighted in Table 9 and the nacelle acceleration computed with the nacelle acceleration root mean square values highlighted in Table 10. The results show that, from a mass minimization point of view, the CHS provided the best configuration. However, for the nacelle acceleration assessment, it is the B-spline curve that yielded the minimum nacelle acceleration value. The nacelle acceleration results are within the allowable limit of 20% to 30% of acceleration due to gravity, according to Rasekhi Nejad et al. [34]; hence, selecting the curve to use requires a trade-off of what criteria are most important to the designer/analyst. To address this trade-off, the TOPSIS ranking procedure is employed to include other criteria assessed in the analysis to rank the curves in their order of importance. This ranking assessment is presented in detail in Section 4.4.5.

**Table 9.** OC3 optimal variant mass for the free-form curves.

| Parametric Curve | B-Spline | CHS | NURBS | Cubic Spline |
|---|---|---|---|---|
| Mass (kg) | 1,893,231 | 1,640,495 | 1,950,902 | 1,792,532 |

**Table 10.** OC3 optimal nacelle acceleration RMS for the free-form curves.

| | CS | CHS | B-Spline | NURBS |
|---|---|---|---|---|
| Nacelle Acceleration RMS ($m/s^2$) | 0.1162 | 0.1105 | 0.1017 | 0.1262 |

A comparison of Tables 6 and 9 shows a reduction in the estimated mass from the OC3 dimensioned modeled spar when optimized variants with a static pitch angle of 5 degrees for all the curves except the NURBS curve were used. Weightage sensitivity of the NURBS curve can potentially lead to a reduction in mass of the optimized variants.

#### 4.4.5. MCDM Assessment—Ranking the Curves

This section highlights the results from the process of using the TOPSIS method to select the parametric free-form curve that is most suitable for modeling the spar platform. The criteria considered are:

- Parametric continuity of curves;
- Computational time (for the shape alteration interfaced MDAO framework to successfully end);
- Estimated mass of selected optimized platform design;
- Shape control capability of the curve;
- Nacelle acceleration response.

The hydrostatic and hydrodynamic analyses to select the optimal design were conducted on a computer system, with the system properties highlighted in Table 11. The properties show that the system used in running the computationally intensive hydrostatic and hydrodynamic analyses is a standard affordable computing system.

**Table 11.** Analysis system specification.

| | |
|---|---|
| System processor | Intel(R) Core(TM) i7-7700 CPU @ 3.60 GHz |
| Operating system | Microsoft Windows 10 |
| Random Access Memory (RAM) | 8.00 GB |
| Storage | 460 GB |
| System type | 64-bit operating system, x64-based processor |

The TOPSIS matrix is provided in Table 12, which represents the key results from the MDAO assessment conducted with the four parametric free-form curves considered. The values within the matrix in Table 12 are the computational time in seconds, estimated mass in kilograms and the motion response culminating in the nacelle acceleration in $m/s^2$ from the MDAO assessment, while the criteria values of shape control and parametric continuity are based on the beneficial advantages on the design curve—a score of two represents a high design advantage and score of one represents little or no advantage on the curve. A detailed analysis of the TOPSIS process is presented in Appendix A. For this study, six random scenarios corresponding to different weightages, as highlighted in Table 13, are considered to estimate the performance values and subsequent ranking of the free-form curves.

**Table 12.** TOPSIS matrix data.

| | **Computational Time (s)** | **Estimated Mass (kg)** | **Shape Control** | **Parametric Continuity** | **Nacelle RMS ($m/s^2$)** |
|---|---|---|---|---|---|
| Optimized B-Spline | 115,417 | 1,893,231 | 2 | 2 | 0.1017 |
| Optimized CHS | 125,083 | 1,640,495 | 1 | 1 | 0.1105 |
| Optimized NURBS | 162,544 | 1,950,902 | 2 | 2 | 0.1262 |
| Optimized Cubic Spline | 132,355 | 1,792,532 | 2 | 2 | 0.1162 |
| $\sum_{j=1}^{n} x_y^2$ | 237,550 | 18,204,272 | 3.6055513 | 3.6055513 | 0.2279957 |

**Table 13.** Scenarios for criteria weightage matrix.

| | **Weightages** | | | | |
|---|---|---|---|---|---|
| | **Computational Time** | **Estimated Mass** | **Shape Control** | **Parametric Continuity** | **Nacelle RMS** |
| Scenario 1 | 1 | 1 | 1 | 1 | 1 |
| Scenario 2 | 1 | 2 | 0.5 | 1 | 2 |
| Scenario 3 | 1 | 0.5 | 2 | 2 | 1 |
| Scenario 4 | 2 | 1 | 0.5 | 0.5 | 1 |
| Scenario 5 | 2 | 2 | 1 | 1 | 0.5 |
| Scenario 6 | 1 | 2 | 1 | 1 | 2 |

The matrix obtained when the weightage has been multiplied by the normalized performance value is the weightage-normalized decision matrix. This is highlighted in Tables 14–19, representing scenarios one to six highlighted in Table 13. For the different scenarios considered, the ideal best and ideal worst values for each criterion were determined taking into consideration if the criteria are classed as beneficial criteria or non-beneficial criteria. The rule is that for beneficial criteria, the highest value is selected, and the least value is selected for non-beneficial criteria. The ideal best and ideal worst values are located

on the last two rows of the scenarios considered in Tables 14–19. The Euclidian distance from the ideal best solution and the ideal worst solution is estimated for all the weightage scenarios assessed and the performance score is derived with the Euclidian distance from the ideal best and ideal worst solutions. The performance ranking of the parametric curves used for the design, analysis and optimization of the OC3 substructure is based on the estimated performance score assessed for all the weighted scenarios considered as highlighted in Tables 14–19.

Table 14 is the weightage-normalized decision matrix that corresponds to scenario one with a baseline weightage of one applied across all the criteria assessed. Table 14 shows that the performance score which is the ratio of the ratio of the Euclidian distance from the ideal worst solution to the summation of the Euclidian distance from the ideal worst solution and the Euclidian distance from the ideal best solution is ranked highest for the B-spline curve. The optimized B-spline curve model performance is closely followed by the optimized cubic spline model performance while the optimized NURBS curve performance is ranked third and the optimized cubic Hermite spline model is ranked as the least performing curve.

In scenarios two, three, five and six, which correspond to Tables 15, 16, 18 and 19, respectively, various subjective weightages as shown in Table 13 are applied across the five criteria to determine the weightage-normalized decision matrix which is used in estimating the performance of the curves. The performance of the curves in Tables 15, 16, 18 and 19 shows the same ranking as highlighted in Table 14, with the B-spline performing best, followed by the cubic spline, the NURBS and lastly the cubic Hermite spline.

Scenario four, which corresponds to Table 17, also with a random subjective weightage applied across the five criteria to estimate the performance of the curves, shows that the best performing curve remains the B-spline and is closely followed by the cubic spline. However, the cubic Hermite spline performed better than the NURBS curve in Table 17 as a result of the weightage used in scenario four. To eliminate the subjectiveness of the applied weightage, it is recommended to integrate the Analytical Hierarchy Process (AHP) for weight estimation with TOPSIS.

For all the weighted scenarios assessed, the B-spline free-form curve is the best performing as it is the only curve that outperformed all the other free-form curves. Closely following the B-spline curve is the cubic spline free-form curve as it is the next best performing curve in all of the six random weighted scenarios assessed. In summary, all the assessed free-form curves—B-spline, NURBS, CHS and cubic spline—are capable of altering the geometric shape design of a spar FOWT, meeting the design objective and constraints. However, assessing the design process with the criteria highlighted in Table 20 shows that the B-spline free-form curve is the most efficient parametric curve for the design and optimization of the spar platform used for the FOWT system.

The summary of the free-form curve ranking of each scenario is presented in Table 20. The best three performing curves in Table 20 are the B-spline, the cubic spline and the NURBS curves. This result aligns with the response results obtained in Section 4.4.2 (parametric curves modeling and analysis with OC3 reduced order dimension) and Section 4.4.4 (shape variation and optimization within the MDAO framework).

**Table 14.** Performance ranking from weighted normalized decision matrix—Scenario 1.

| | Computation Time | Estimated Mass | Shape Control | Parametric Continuity | Nacelle RMS | Euclidian Distance from Ideal Best Solution | Euclidian Distance from Ideal Worst Solution | Sum of Euclidian Distances | Performance Score | Ranking |
|---|---|---|---|---|---|---|---|---|---|---|
| Optimized B-Spline | 0.4275 | 0.5192 | 0.5547 | 0.5547 | 0.4461 | 0.0693 | 0.4428 | 0.5122 | 0.8647 | 1 |
| Optimized CHS | 0.4633 | 0.4499 | 0.2774 | 0.2774 | 0.4847 | 0.3957 | 0.1767 | 0.5725 | 0.3087 | 4 |
| Optimized NURBS | 0.6020 | 0.5351 | 0.5547 | 0.5547 | 0.5535 | 0.2219 | 0.3922 | 0.6142 | 0.6386 | 3 |
| Optimized Cubic Spline | 0.4902 | 0.4916 | 0.5547 | 0.5547 | 0.5097 | 0.0986 | 0.4125 | 0.5111 | 0.8071 | 2 |
| Weight | 1.0000 | 1.0000 | 1.0000 | 1.0000 | 1.0000 | | | | | |
| Ideal best solution | 0.4275 | 0.4499 | 0.5547 | 0.5547 | 0.4461 | | | | | |
| Ideal worst solution | 0.6020 | 0.5351 | 0.2774 | 0.2774 | 0.5535 | | | | | |

**Table 15.** Performance ranking from weighted normalized decision matrix—Scenario 2.

| | Computation Time | Estimated Mass | Shape Control | Parametric Continuity | Nacelle RMS | Euclidian Distance from Ideal Best Solution | Euclidian Distance from Ideal Worst Solution | Sum of Euclidian Distances | Performance Score | Ranking |
|---|---|---|---|---|---|---|---|---|---|---|
| Optimized B-Spline | 0.4275 | 1.0385 | 0.2774 | 0.5547 | 0.8921 | 0.1386 | 0.3792 | 0.5178 | 0.7323 | 1 |
| Optimized CHS | 0.4633 | 0.8998 | 0.1387 | 0.2774 | 0.9693 | 0.3216 | 0.2253 | 0.5468 | 0.4119 | 4 |
| Optimized NURBS | 0.6020 | 1.0701 | 0.2774 | 0.5547 | 1.1070 | 0.3250 | 0.3223 | 0.6473 | 0.4979 | 3 |
| Optimized Cubic Spline | 0.4902 | 0.9832 | 0.2774 | 0.5547 | 1.0193 | 0.1645 | 0.3409 | 0.5054 | 0.6745 | 2 |
| Weight | 1.0000 | 2.0000 | 0.5000 | 1.0000 | 2.0000 | | | | | |
| Ideal best solution | 0.4275 | 0.8998 | 0.2774 | 0.5547 | 0.8921 | | | | | |
| Ideal worst solution | 0.6020 | 1.0701 | 0.1387 | 0.2774 | 1.0193 | | | | | |

**Table 16.** Performance ranking from weighted normalized decision matrix—Scenario 3.

| | Computation Time | Estimated Mass | Shape Control | Parametric Continuity | Nacelle RMS | Euclidian Distance from Ideal Best Solution | Euclidian Distance from Ideal Worst Solution | Sum of Euclidian Distances | Performance Score | Ranking |
|---|---|---|---|---|---|---|---|---|---|---|
| Optimized B-Spline | 0.4275 | 0.2596 | 1.1094 | 1.1094 | 0.4461 | 0.0347 | 0.8062 | 0.8409 | 0.9588 | 1 |
| Optimized CHS | 0.4633 | 0.2250 | 0.5547 | 0.5547 | 0.4847 | 0.7862 | 0.1473 | 0.9335 | 0.1578 | 4 |
| Optimized NURBS | 0.6020 | 0.2675 | 1.1094 | 1.1094 | 0.5535 | 0.2093 | 0.7857 | 0.9950 | 0.7896 | 3 |
| Optimized Cubic Spline | 0.4902 | 0.2458 | 1.1094 | 1.1094 | 0.5097 | 0.0917 | 0.7927 | 0.8844 | 0.8963 | 2 |
| Weight | 1.0000 | 0.5000 | 2.0000 | 2.0000 | 1.0000 | | | | | |
| Ideal best solution | 0.4275 | 0.2250 | 1.1094 | 1.1094 | 0.4461 | | | | | |
| Ideal worst solution | 0.6020 | 0.2675 | 0.5547 | 0.5547 | 0.5097 | | | | | |

**Table 17.** Performance ranking from weighted normalized decision matrix—Scenario 4.

| | Computation Time | Estimated Mass | Shape Control | Parametric Continuity | Nacelle RMS | Euclidian Distance from Ideal Best Solution | Euclidian Distance from ideal Worst Solution | Sum of Euclidian Distances | Performance Score | Ranking |
|---|---|---|---|---|---|---|---|---|---|---|
| Optimized B-Spline | 0.8549 | 0.5192 | 0.2774 | 0.2774 | 0.4461 | 0.0693 | 0.4149 | 0.4842 | 0.8568 | 1 |
| Optimized CHS | 0.9265 | 0.4499 | 0.1387 | 0.1387 | 0.4847 | 0.2123 | 0.2983 | 0.5106 | 0.5842 | 3 |
| Optimized NURBS | 1.2040 | 0.5351 | 0.2774 | 0.2774 | 0.5535 | 0.3750 | 0.1961 | 0.5712 | 0.3434 | 4 |
| Optimized Cubic Spline | 0.9804 | 0.4916 | 0.2774 | 0.2774 | 0.5097 | 0.1467 | 0.3038 | 0.4505 | 0.6743 | 2 |
| Weight | 2.0000 | 1.0000 | 0.5000 | 0.5000 | 1.0000 | | | | | |
| Ideal best solution | 0.8549 | 0.4499 | 0.2774 | 0.2774 | 0.4461 | | | | | |
| Ideal worst solution | 1.2040 | 0.5351 | 0.1387 | 0.1387 | 0.5535 | | | | | |

**Table 18.** Performance ranking from weighted normalized decision matrix—Scenario 5.

| | Computation Time | Estimated Mass | Shape Control | Parametric Continuity | Nacelle RMS | Euclidian Distance from Ideal Best Solution | Euclidian Distance from Ideal Worst Solution | Sum of Euclidian Distances | Performance Score | Ranking |
|---|---|---|---|---|---|---|---|---|---|---|
| Optimized B-Spline | 0.8549 | 1.0385 | 0.5547 | 0.5547 | 0.2230 | 0.1386 | 0.5288 | 0.6674 | 0.7923 | 1 |
| Optimized CHS | 0.9265 | 0.8998 | 0.2774 | 0.2774 | 0.2423 | 0.3992 | 0.3274 | 0.7265 | 0.4506 | 4 |
| Optimized NURBS | 1.2040 | 1.0701 | 0.5547 | 0.5547 | 0.2768 | 0.3921 | 0.3922 | 0.7843 | 0.5001 | 3 |
| Optimized Cubic Spline | 0.9804 | 0.9832 | 0.5547 | 0.5547 | 0.2548 | 0.1540 | 0.4603 | 0.6143 | 0.7493 | 2 |
| Weight | 2.0000 | 2.0000 | 1.0000 | 1.0000 | 0.5000 | | | | | |
| Ideal best solution | 0.8549 | 0.8998 | 0.5547 | 0.5547 | 0.2230 | | | | | |
| Ideal worst solution | 1.2040 | 1.0701 | 0.2774 | 0.2774 | 0.2768 | | | | | |

**Table 19.** Performance ranking from weighted normalized decision matrix—Scenario 6.

| | Computation Time | Estimated Mass | Shape Control | Parametric Continuity | Nacelle RMS | Euclidian Distance from Ideal Best Solution | Euclidian Distance from Ideal Worst Solution | Sum of Euclidian Distances | Performance Score | Ranking |
|---|---|---|---|---|---|---|---|---|---|---|
| Optimized B-Spline | 0.4275 | 1.0385 | 0.5547 | 0.5547 | 0.8921 | 0.1386 | 0.4489 | 0.5875 | 0.7640 | 1 |
| Optimized CHS | 0.4633 | 0.8998 | 0.2774 | 0.2774 | 0.9693 | 0.4014 | 0.2253 | 0.6266 | 0.3595 | 4 |
| Optimized NURBS | 0.6020 | 1.0701 | 0.5547 | 0.5547 | 1.1070 | 0.3250 | 0.4019 | 0.7269 | 0.5529 | 3 |
| Optimized Cubic Spline | 0.4902 | 0.9832 | 0.5547 | 0.5547 | 1.0193 | 0.1645 | 0.4170 | 0.5815 | 0.7171 | 2 |
| Weight | 1.0000 | 2.0000 | 1.0000 | 1.0000 | 2.0000 | | | | | |
| Ideal best solution | 0.4275 | 0.8998 | 0.5547 | 0.5547 | 0.8921 | | | | | |
| Ideal worst solution | 0.6020 | 1.0701 | 0.2774 | 0.2774 | 1.0193 | | | | | |

**Table 20.** Summary of curve ranking.

| | Ranking | | | |
|---|---|---|---|---|
| | **1st** | **2nd** | **3rd** | **4th** |
| Scenario 1 | B-spline | Cubic Spline | NURBS | CHS |
| Scenario 2 | B-spline | Cubic Spline | NURBS | CHS |
| Scenario 3 | B-spline | Cubic Spline | NURBS | CHS |
| Scenario 4 | B-spline | Cubic Spline | CHS | NURBS |
| Scenario 5 | B-spline | Cubic Spline | NURBS | CHS |
| Scenario 6 | B-spline | Cubic Spline | NURBS | CHS |

## 5. Conclusions and Recommendation

This study investigates the use of different parametric free-form curves for the design, analysis and optimization of the spar platform of an NREL 5 MW floating offshore wind turbine. The parametric free-form curves investigated are the cubic spline, the CHS, the B-spline and the NURBS curve. These curves were used to model and optimize a spar platform for floating wind turbines based on the NREL OC3 spar platform's dimensions. The hydrodynamics assessment was conducted with the potential flow theory approach in the frequency domain to estimate the response amplitude operator of the system. Each parametric curve was integrated within an MDAO framework using the DNV Sesam GeniE 64 V8.4-06 and HydroD 64 v6.1-02 plus in-house programming and data analysis codes to interface the different disciplines.

The objective function within the MDAO framework is to minimize the mass of steel used in the design. The main constraint is to ensure that the maximum pitch angle of inclination of the system does not exceed 5 degrees. The results from the MDAO framework satisfying the objective function and constraints are assessed with the TOPSIS MCDM technique to determine the best performing curve using different marking criteria such as the computational time, designed mass of the platform, nacelle acceleration and properties of the free-form curve (shape control capability and parametric continuity of the curve).

Different scenarios were considered by varying the weighting of each marking criteria of the TOPSIS analysis conducted. A defined trend with all the scenarios assessed is that the best parametric curve approach is the B-spline curve while the worst one is the CHS. This result is highly impacted by criteria such as mass, computational time parametric continuity and shape control properties. As observed from the response assessment from the MDAO framework, the TOPSIS MCDM ranking of the free-form curve's outcome is not so much impacted by the response as the peak response frequencies in surge, heave and pitch degrees of freedom for all the four free-form curves assessed (cubic spline, B-Spline, NURBS and cubic Hermite spline) occur outside or just circa the boundary of the first-order wave excitation frequency range of 5 s to 25 s. This study shows that the use of the TOPSIS technique to prove the B-spline is a more effective parameterization curve to use for modeling within an MDAO framework. The shape alteration of the optimized floaters can also lead to a reduction in mass of the floater, leading to a reduction in the capital cost of steel required for manufacturing.

This study allows the exploration of practical concepts in order to make the FOWT sector as competitive as the fixed bottom offshore wind turbine sector because the innovative geometric shapes generated from the free-form curves assessed within the optimization study can help reduce the cost of the floating platform with a strong potential to reduce the levelized cost of energy. The findings of this study can lead to the design, optimization and manufacturing of innovative platforms with the potential for an improved hydrodynamic response in comparison to the traditional platform concepts from the oil and gas sector, predominantly the early-to-market platforms currently in used in the FOWT sector.

In addition to the parametric curve comparison for modeling substructures of FOWTs as highlighted in this article, it is recommended to explore more free-form curves. Free-form curves like polygon curves, polyline, T-Spline and alternative parametrization techniques like free-form deformation and the CAD method can be explored for a more effective approach to modeling innovative FOWT substructures. It is also recommended to determine the weighted normalized decision matrix from weights estimated using the non-subjective Analytic Hierarchy Process method. Refining the weightage of the NURBS curve for optimal geometry is an essential sensitivity study recommended to advance this research as NURBS curves have been widely used in the field of approximating data and their fitting accuracy can be increased by adjusting the values of their weights. It is expected that the accuracy of the NURBS curve with adequate weightage will be reflected in the rankings of the curves assessed.

A limitation that is anticipated with the bespoke shapes of the platform selected from this study is the manufacturing difficulty in producing them. However, ongoing research in the manufacturing and development of wire arc additive manufacturing (WAAM) capabilities—3D printing of metals and concrete slip-forming—are anticipated to help navigate this limitation.

**Author Contributions:** Article structure and conceptualization, A.O., M.C. and A.C.; parameterization software, A.O.; data curation, A.O.; optimization framework, A.O., M.C. and A.C.; analyses and investigation, A.O. and M.C.; writing—original draft preparation, A.O.; writing—review and editing, M.C. and A.C.; project supervision, M.C. and A.C. All authors have read and agreed to the published version of the manuscript.

**Funding:** This work is conducted with the Renewable Energy Marine Structures (REMS) group at the University of Strathclyde and the funding is provided by the Engineering and Physical Sciences Research Council (EPSRC) UK (Grant No: EP/L016303/1).

**Data Availability Statement:** Not applicable.

**Conflicts of Interest:** The authors declare no conflict of interest.

## Abbreviations

| | |
|---|---|
| B-Spline | Basis Spline |
| CHS | Cubic Hermite Spline |
| DNV | Det Norske Veritas |
| DLC | Dynamic Load Case |
| DOF | Degree of Freedom |
| FEM | Finite Element Method |
| FOWT | Floating Offshore Wind Turbine |
| GB | Gradient Based |
| GF | Gradient Free |
| JONSWAP | Joint North Sea Wave Project |
| MDAO | Multidisciplinary Design Analysis and Optimization |
| MCDM | Multi Criteria Decision Making |
| NURBS | Non-Uniform Rational B-Spline |
| OC3 | Offshore Code Comparison Collaboration |
| OWT | Offshore Wind Turbine |
| PSM | Pattern Search Model |
| RAO | Response Amplitude Operator |
| RMS | Root Mean Square |
| RNA | Rotor Nacelle Assembly |
| SQP | Sequential Quadratic Programming |
| TOPSIS | Technique for Order of Preference by Similarity to Ideal Solution |
| TLP | Tension-Leg Platform |
| WADAM | Wave Analysis by Diffraction and Morison Theory |

## Appendix A. TOPSIS Process

The TOPSIS process from Section 3.2 is detailed herein. The steps applied in Figure 2 are highlighted below:

1. Define criteria, options and attributes used in selection of optimal process.
2. Obtain a decision matrix using selected input data of design options and criteria $x_{i,j}$, where i = 1 ... m represents the design options and j = 1 ... n represents the design criteria.
3. Normalize the decision matrix along each column. This is conducted by dividing each cell within the matrix by the summation of the square of all cells within the matrix column of interest. The decision matrix is derived as highlighted in Equation (A1).

$$r_{i,j} = \frac{x_{i,j}}{\sqrt{\sum_{j=1}^{m} x_{i,j}^2}} \tag{A1}$$

4. Apply the relative weighing factor to the normalized matrix considering the characterization of the variables as positive or negative as highlighted in Equation (A2).

$$v_{i,j} = w_j r_{i,j} \tag{A2}$$

5. Define the best and worst alternative for each of the weighing vectors within the weightage-normalized decision matrix.
6. Calculate the ideal maximum and minimum values for each column with the set of equations shown in Equation (A3).

$$x_{i,j}^{+} = \max_{1 \le j \le n} (x_{i,j}) \text{ and } x_{i,j}^{-} = \min_{1 \le j \le n} (x_{i,j}) \tag{A3}$$

The relative distances from the positive and negative ideal solutions can be estimated using the n-dimensional equivalent of Pythagoras' theorem as described with the expressions shown in Equation (A4).

$$\begin{gathered} D_i^{+} = \sqrt{\sum_{j=1}^{m} \left(a_{ij}^{+} - a_{ij}\right)^2} \\ \text{and} \\ D_i^{-} = \sqrt{\sum_{j=1}^{m} \left(a_{ij}^{-} - a_{ij}\right)^2} \end{gathered} \tag{A4}$$

7. Estimate the rating for ranking the results based on their overall performance with the expression in Equation (A5)

$$C_i = \frac{D_I^{-}}{D_i^{-} + D_i^{+}} \tag{A5}$$

The best design option or solution selected is the one that is both far from the negative ideal solution and close to the positive ideal solution, deriving the highest score.

## References


1. Zheng, X.Y.; Lei, Y. Stochastic response analysis for a floating offshore wind turbine integrated with a steel fish farming cage. *Appl. Sci.* **2018**, *8*, 1229. [CrossRef]
2. Heronemus, W.E. Pollution-Free Energy from the Offshore Winds. In Proceedings of the 8th Annual Conference and Exposition, Marine Technology Society, Washington, DC, USA, 11–13 September 1972.
3. Tracy, C.H. Parametric Design of Floating Wind Turbines. Ph.D. Thesis, Massachusetts Institute of Technology, Cambridge, MA, USA, 2007.
4. Rahmdel, S.; Wang, B.; Han, C.; Kim, K.; Park, S. A parametric study of spar-type floating offshore wind turbines (FOWTs) by numerical and experimental investigations. *Ships Offshore Struct.* **2016**, *11*, 818–832. [CrossRef]
5. Hegseth, J.M.; Bachynski, E.E.; Martins, J.R. Integrated design optimization of spar floating wind turbines. *Mar. Struct.* **2020**, *72*, 102771. [CrossRef]
6. Birk, L. Parametric modeling and shape optimization of offshore structures. *Int. J. CAD/CAM* **2006**, *6*, 29–40.

7. Katsoulis, T.; Wang, X.; Kaklis, P.D. A T-splines-based parametric modeller for computer-aided ship design. *Ocean Eng.* **2019**, *191*, 106433. [CrossRef]
8. Hall, M.; Buckham, B.; Crawford, C. Evolving offshore wind: A genetic algorithm-based support structure optimization framework for floating wind turbines. In Proceedings of the OCEANS 2013 MTS/IEEE Bergen: The Challenges of the Northern Dimension, Bergen, Norway, 10–14 June 2013; IEEE: Piscataway, NJ, USA, 2013.
9. Karimi, M.; Hall, M.; Buckham, B.; Crawford, C. A multi-objective design optimization approach for floating offshore wind turbine support structures. *J. Ocean Eng. Mar. Energy* **2017**, *3*, 69–87. [CrossRef]
10. Ramsay, W.; Goupee, A.; Allen, C.; Viselli, A.; Kimball, R. Optimization of a Lightweight Floating Offshore Wind Turbine with Water Ballast Motion Mitigation Technology. *Wind* **2022**, *2*, 535–570. [CrossRef]
11. Dou, S.; Pegalajar-Jurado, A.; Wang, S.; Bredmose, H.; Stolpe, M. Optimization of floating wind turbine support structures using frequency-domain analysis and analytical gradients. *J. Phys. Conf. Ser.* **2020**, *1618*, 042028. [CrossRef]
12. Ojo, A.; Collu, M.; Coraddu, A. Parametrisation Scheme for Multidisciplinary Design Analysis and Optimisation of a Floating Offshore Wind Turbine Substructure—OC3 5MW Case Study. *J. Phys. Conf. Ser.* **2022**, *2265*, 042009. [CrossRef]
13. Caylor, J.P.; Hanratty, T.P. *Survey of Multi Criteria Decision Making Methods for Complex Environments*; CCDC Army Research Laboratory: Adelphi, MD, USA, 2020.
14. Roszkowska, E. Multi-criteria decision making models by applying the TOPSIS method to crisp and interval data. *Mult. Criteria Decis. Mak./Univ. Econ. Katow.* **2011**, *6*, 200–230.
15. Kolios, A.J.; Rodriguez-Tsouroukdissian, A.; Salonitis, K. Multi-criteria decision analysis of offshore wind turbines support structures under stochastic inputs. *Ships Offshore Struct.* **2016**, *11*, 38–49.
16. Leimeister, M.; Kolios, A. A review of reliability-based methods for risk analysis and their application in the offshore wind industry. *Renew. Sustain. Energy Rev.* **2018**, *91*, 1065–1076. [CrossRef]
17. Leimeister, M.; Kolios, A.; Collu, M. Critical review of floating support structures for offshore wind farm deployment. *J. Phys. Conf. Ser.* **2018**, *1104*, 1–11. [CrossRef]
18. Lozano-Minguez, E.; Kolios, A.J.; Brennan, F.P. Multi-criteria assessment of offshore wind turbine support structures. *Renew. Energy* **2011**, *36*, 2831–2837. [CrossRef]
19. Goldman, R.A. (Ed.) Dynamic Programming Approach to Curves and Surfaces for Geometric Modeling. In *Pyramid Algorithms*; Morgan Kaufmann: San Francisco, CA, USA, 2003; pp. 1–43.
20. McClarren, R.G. (Ed.) Chapter 10—Interpolation. In *Computational Nuclear Engineering and Radiological Science Using Python*; Academic Press: Cambridge, MA, USA, 2018; pp. 173–192.
21. Biran, A. (Ed.) Chapter 7—Cubic Splines. In *Geometry for Naval Architects*; Butterworth-Heinemann: Oxford, UK, 2019; pp. 305–324.
22. Farin, G. (Ed.) *Curves and Surfaces for Computer-Aided Geometric Design Curves and Surfaces for Computer-Aided Geometric Design*; Academic Press: New York, NY, USA, 1990.
23. Li, J.; Liu, C. Cubic Trigonometric Hermite Interpolation Curve: Construction, Properties, and Shape Optimization. *J. Funct. Spaces* **2022**, *2022*, 7525056. [CrossRef]
24. Dimas, E.; Briassoulis, D. 3D geometric modelling based on NURBS: A review. *Adv. Eng. Softw.* **1999**, *30*, 741–751. [CrossRef]
25. Samareh, J.A. Survey of shape parameterization techniques for high-fidelity multidisciplinary shape optimization. *AIAA J.* **2001**, *39*, 877–884. [CrossRef]
26. Hwang, C.-L.; Yoon, K. (Eds.) Methods for Multiple Attribute Decision Making. In *Multiple Attribute Decision Making: Methods and Applications a State-of-the-Art Survey*; Springer: Berlin/Heidelberg, Germany, 1981; pp. 58–191.
27. Jonkman, J.M. *Definition of the Floating System for Phase IV of OC3*; National Renewable Energy Lab.(NREL): Golden, CO, USA, 2010.
28. Leimeister, M.; Kolios, A.; Collu, M.; Thomas, P. Design optimization of the OC3 phase IV floating spar-buoy, based on global limit states. *Ocean Eng.* **2020**, *202*, 107186. [CrossRef]
29. DNV. Sesam Feature Description. Software Suite for Hydrodynamic and Structural Analysis of Renewable, Offshore and Maritime Structures. 2021. Available online: https://www.dnv.com/Images/Sesam-Feature-Description_tcm8-58834.pdf (accessed on 29 November 2021).
30. Jonkman, J.M. *Dynamics Modeling and Loads Analysis of an Offshore Floating Wind Turbine*; University of Colorado at Boulder: Boulder, CO, USA, 2007.
31. Journée, J.M.J.; Massie, W.W. *Offshore Hydromechanics*, 1st ed.; Delft University of Technology: Delft, The Netherlands, 2000; p. 570.
32. Newman, J.N. *Marine Hydrodynamics*; The MIT Press: Cambridge, MA, USA, 2018; p. 450.
33. Palacio-Morales, J.; Tobón, A.; Herrera, J. Optimization Based on Pattern Search Algorithm Applied to pH Non-Linear Control: Application to Alkalinization Process of Sugar Juice. *Processes* **2021**, *9*, 2283. [CrossRef]
34. Rasekhi Nejad, A.; Bachynski, E.E.; Moan, T. On Tower Top Axial Acceleration and Drivetrain Responses in a Spar-Type Floating Wind Turbine. In Proceedings of the ASME 2017 36th International Conference on Ocean, Offshore and Arctic Engineering, Trondheim, Norway, 25–30 June 2017.


**Disclaimer/Publisher's Note:** The statements, opinions and data contained in all publications are solely those of the individual author(s) and contributor(s) and not of MDPI and/or the editor(s). MDPI and/or the editor(s) disclaim responsibility for any injury to people or property resulting from any ideas, methods, instructions or products referred to in the content.